LAWRENCE
LIVERMORE
NATIONAL
LABORATORY

UCRL-CONF-222137

SHOCK INITIATION EXPERIMENTS AND MODELING OF COMPOSITION B AND C-4

Paul A. Urtiew, Kevin S. Vandersall, Craig M. Tarver, Frank Garcia, Jerry W. Forbes

June 16, 2006

13th International Detonation Symposium
Norfolk, VA, United States
July 23, 2006 through July 28, 2006

SHOCK INITIATION EXPERIMENTS AND MODELING OF COMPOSITION B AND C-4

Paul A. Urtiew[1], Kevin S. Vandersall[1], Craig M. Tarver[1], Frank Garcia[1], and Jerry W. Forbes[2]

[1]Energetic Materials Center, Lawrence Livermore National Laboratory, Livermore, CA 94550
[2]Center for Energetic Concepts Development, University of Maryland, College Park, MD 20742

Abstract. Shock initiation experiments on the explosives Composition B and C-4 were performed to obtain in-situ pressure gauge data for the purpose of determining the Ignition and Growth reactive flow model with proper modeling parameters. A 101 mm diameter propellant driven gas gun was utilized to initiate the explosive charges containing manganin piezoresistive pressure gauge packages embedded in the explosive sample. Experimental data provided new information on the shock velocity versus particle velocity relationship for each of the investigated materials in their respective pressure range. The run-distance-to-detonation points on the Pop-plot for these experiments showed agreement with previously published data, and Ignition and Growth modeling calculations resulted in a good fit to the experimental data. These experimental data were used to determine Ignition and Growth reactive flow model parameters for these explosives. Identical ignition and growth reaction rate parameters were used for C-4 and Composition B, and the Composition B model also included a third reaction rate to simulate the completion of reaction by the TNT component. The Composition B model was then tested on existing short pulse duration, gap test, and projectile impact shock initiation with good results. This Composition B model can be applied to shock initiation scenarios that have not or cannot be tested experimentally with a high level of confidence in its predictions.

INTRODUCTION

Shock initiation is one of the most important properties of energetic materials (EM), which determines whether or not the material will build up in pressure after being shocked and eventually transit to a full-fledged detonation or if it will die out before it gains strength from induced reaction. Study of this property is important to gain knowledge of when the material will detonate as intended when intentionally shocked and, at the same time, when it will not detonate when it is accidentally exposed to dynamic loading.

Energetic materials are widely used in both industrial applications and at defense oriented establishments. However, some of the most common energetic materials are also used for ill intent. Therefore, initiation of such materials is of particular interest for reasons of safety and understanding of their behavior under dynamic loading conditions.

In earlier publications we have reported initiation thresholds for build up to detonation and sensitivity to impact (Pop-plots) of both sensitive and insensitive HMX and TATB based explosives at various initial temperatures.[1,2] In this publication we will report on initiation and sensitivity of more common RDX based explosives known as C-4 and Composition B. This work will provide previously unpublished manganin gauge records for sustained pulse shock initiation and will compliment it with modeling short shock pulse shock initiation experiments by Trott and Jung;[3] embedded particle velocity gauge detonation experiments by Cowperthwaite and Rosenberg;[4] and failure diameter / detonation wave curvature

experiments by Campbell and Engelke.[5] This reactive flow model uses one reaction growth rate for the RDX component of Composition B and another reaction growth rate for the TNT. Similar models for mixtures, such RX-26-AF, which is approximately half HMX and half TATB, have been used in this manner successfully.[6]

EXPERIMENTAL TECHNIQUE

The Shock Initiation experiments were performed on the 101 mm bore, propellant driven gas gun, which allows precise control of the projectile velocity and of the loading pressure imposed on the energetic material target. The experimental set-up is illustrated in Fig 1.

There were two types of target assemblies that were used in these experiments. One target assembly consisted of several discs of different thicknesses. Gauge packages containing manganin pressure gauges were embedded between individual discs. The other target assembly consisted of two 24˚ wedges with one multi-element pressure gage package placed between them. The intent here was to eliminate the effect of inert package material on each consecutive gauge element. The gauges are armored with thin (125 μm) Teflon insulation on both sides to prevent shorting of the gauges in a conductive medium when the material becomes reactive. Other details of the manganin pressure gauges are described in our previous publications.[7,8]

For better control of the impact pressure, a thin buffer plate of the same material as the impact plate is placed in front of the target assembly for symmetrical impact. Also included in the two target assemblies are six tilt pins placed around the periphery of the target flush with the impact surface to measure the tilt of the impact plate as it strikes the target, and four velocity pins sticking out some known distance from the target to measure the velocity of the impact plate just before it strikes the target.

During the experiment, oscilloscopes measure change of voltage as result of resistance change in the gauges which were then converted to pressure using the hysteresis corrected calibration curve published elsewhere.[9] From the data of the shock arrival times of the gauge locations, a plot of distance vs. time ("x-t plot") is constructed with the slope of the plotted lines yielding the shock velocities with two lines apparent, a line for the un-reacted state as it reacts and a line representing the detonation velocity. The intersection of these two lines is taken as the "run-distance-to-detonation," which is then plotted on the "Pop-Plot" showing the run-distance-to-detonation as a function of the input pressure in log-log space.

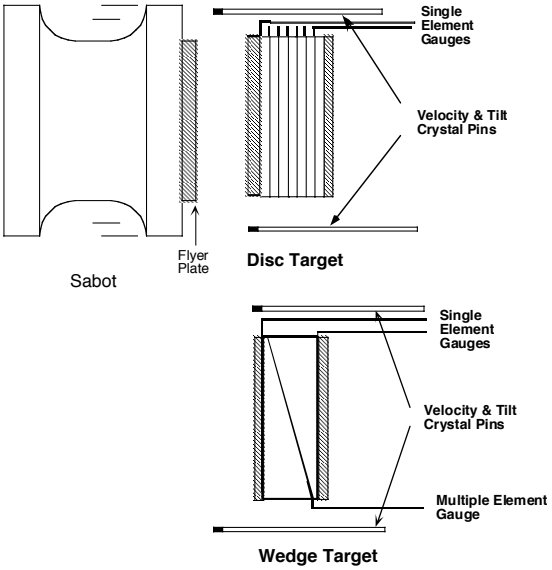

Figure 1. Schematic diagram of experimental set-up for gun experiments.

Table 1. Listing of Shock Initiation Gun Experiments

Shot #	Target	Velocity (km/s)	Pressure (GPa)	Dist. to Det. (mm)
4565	C-4	0.600	2.20	25
4547	C-4	0.737	2.86	17
4564	C-4	0.987	4.20	9
4359	Comp. B	0.835	3.78	16
4544	Comp. B	0.929	4.35	12
4540	Comp. B	1.005	4.80	10
4545	Comp. B	1.307	6.84	5

EXPERIMENTAL RECORDS

A total of 7 shots were fired of which 3 of them were with the C-4 explosives in the disc target configuration and 4 with the Composition B in the wedge target configuration. Impact velocities and pressures imposed on the targets material are listed in Table 1.

Figure 2 shows pressure records of a shock loaded RDX-based high explosive C-4 (91 weight % RDX and 9 weight % of other additives) pressed to 98.5% of theoretical maximum density. The explosive samples in these experiments were shock loaded with an aluminum impactor flying at a velocity of 0.6, mm/μs, imposing a pressure on the target

material 2.2 GPa. As in all heterogeneous explosives these traces exhibit the characteristic features of their initiation: some reaction occurs just behind the shock front causing it to grow in pressure, but most of the reaction occurs well behind the leading shock, creating a pressure wave that overtakes the initial shock wave causing the process to finally transit to detonation. In this case the transition to detonation occurred at about 25 mm into the target.

Figure 3 illustrates the records obtained with a wedge type experiments performed on another RDX based explosive Composition B (63-weight % RDX, 36-weight % TNT and 1weight % of Wax) at ambient room temperature. It shows initially a steady shock wave and then, after the reaction becomes significant, a strong growth in pressure just before the transition to detonation. The loading pressure in this experiment was 4.8 GPa.

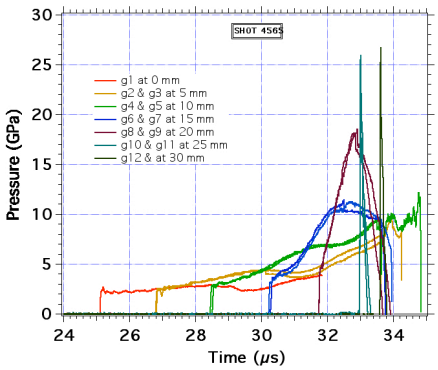

Figure 2. A typical pressure gauge record for the C-4 material.

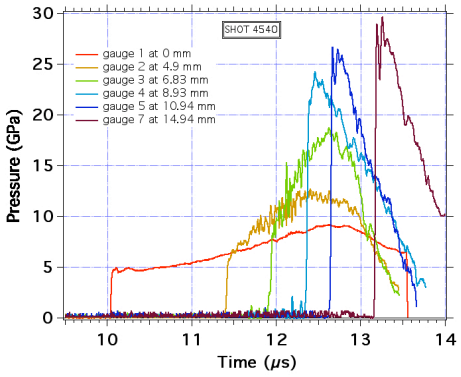

Figure 3. A typical pressure gauge record for the Composition B material.

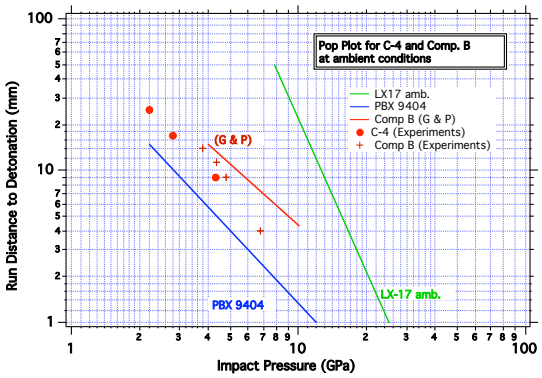

Figure 4. Pop-Plot showing data from C-4 and Composition B along with reference lines.

Shock sensitivity of both C-4 and Composition B for various initial pressures is illustrated in Fig. 4 on a so-called "Pop Plot", which displays the dependence of the distance to detonation on the initial impact pressure. On this plot one can easily compare the relative sensitivity of these explosives to a more sensitive explosive HMX-based PBX 9404 and a TATB based insensitive high explosive LX-17 at their ambient conditions. On a log-log plot the run distance to detonation versus shock pressure these data mostly fall on a straight line. The closer the line is to the origin of the plot, the more sensitive is the material. Shown here are also previously published data of Gibbs and Popolato.[10]

EQUATION OF STATE ANALYSIS

For any new material that was tested in our laboratory we also determine their experimental equation of state in the form of a new shock velocity versus particle velocity (U_s-u_p) relationship. This analysis is done by using the well-known impedance matching technique and is illustrated in Figures 5 and 6 for the case of C-4 and Comp B respectively.

Assuming that the EOS relations of the impactor at room temperature are very well known, one can plot the inverse adiabat of the flyer plate originating at the flyer velocity. Experimental measurement of the initial pressure from several experiments will result in the adiabat of the new target material. Measured shock velocities between the first two or more gauge stations from the same experiments allow one to draw a line through the experimental points in the shock velocity – mass velocity plane and determine the new U_s-u_p relationship for this material.

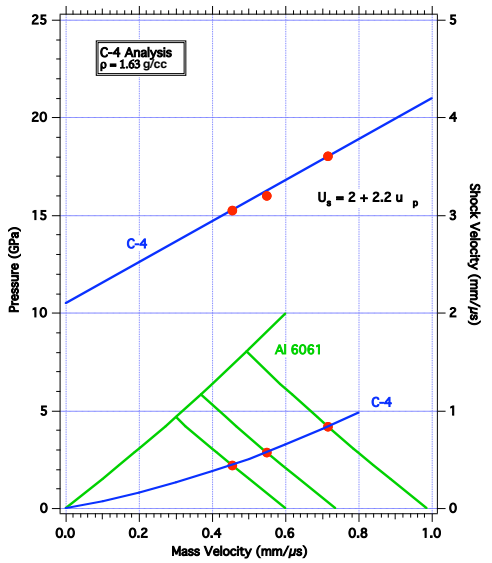

Figure 5. Impedance matching and U_S-u_P for C-4.

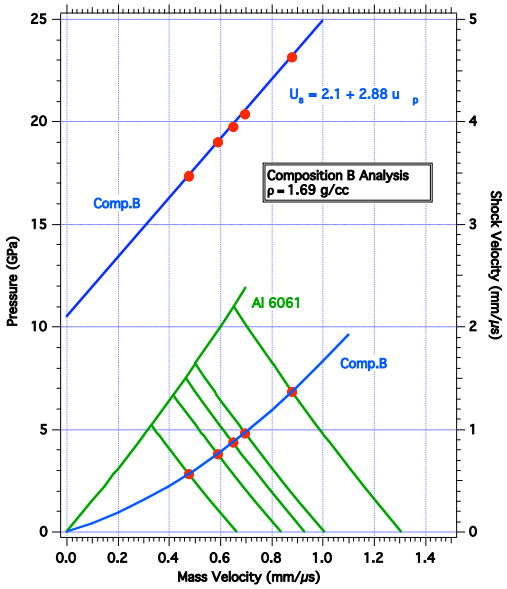

Figure 6. Impedance matching and U_S-u_P for Composition B.

IGNITION & GROWTH MODELING

The Ignition and Growth reactive flow model for shock initiation and detonation is described in detail in a companion paper.[11] Since the embedded pressure gauges require one-dimensional flow, the calculations are also one-dimensional and use a mesh size of 50 zones per mm. Since both C-4 and Comp B are RDX-based, they exhibit similar early hot spot formation and growth rates. Thus, the first and second reaction rates are normalized to the C-4 embedded gauge records and then used to model the Comp B records. Since Comp B has been demonstrated to undergo shock desensitization in certain situations,[12] a value of 0.0367 for the critical compression parameter in the Ignition rate law was used to prevent ignition below approximately 0.5 GPa. The third reaction rate is used to describe the slower reaction of the TNT component of Comp B. Comp B contains approximately 60% RDX, but, since RDX is more energetic than TNT, 70% of the chemical energy is assumed to be liberated at the RDX reaction rates and 30% by the TNT rates. Separating the reaction rates in this manner has been used successfully in previous modeling efforts in which two materials react at sufficiently different rates. Examples include RX-26-AF, which contains half HMX and half TATB,[13] and various aluminized explosives, in which aluminum is oxidized by previously formed explosive reaction product gases.[14] In the following sections, Ignition and Growth calculations are compared to the measured pressure histories and run distances to detonation for C-4 and Comp B. The Comp B model is compared to short shock pulse duration experiments, several gap test results, and two recent studies of shock initiation of bare and covered Comp B charges by brass and steel projectiles.

Table 2. Ignition & Growth parameters for C-4.

UNREACTED JWL	PRODUCT JWL
A=778.1 Mbar	A=6.0977 Mbar
B=-0.05031 Mbar	B=0.1295 Mbar
R_1=11.3	R_1=4.5
R_2=1.13	R_2=1.4
ω=0.8938	ω=0.25
C_V=2.487x10^{-5} Mbar/K	C_V=1.0x10^{-5} Mbar/K
T_O = 298°K	E_O=0.09 Mbar
Shear Modulus=0.0354 Mbar	-
Yield Strength=0.002 Mbar	-
ρ_0=1.601 g/cm^3	-
REACTION RATES	
a=0.0367	x=7.0
b=0.667	y=2.0
c=0.667	z=3.0
d=0.333	F_{igmax}=0.022
e=0.667	F_{G1max}=1.0
g=0.667	F_{G2min} =0.0
I=1.4 x 10^{11} μs^{-1}	G_1=140 Mbar^{-2}μs^{-1}
-	G_2=0.0 Mbar^{-2}μs^{-1}

Table 3. Gruneisen equation of state parameters for the inert materials using the following equation: $P = \rho_o c^2 \mu[1+(1-\gamma_o/2)\mu - a/2\mu^2]/[1-(S_1-1)\mu - S_2\mu^2/(\mu+1) - S_3\mu^3/(\mu+1)^2]^2 + (\gamma_o + a\mu)E$, where $\mu = (\rho/\rho_o - 1)$ and E is thermal energy.

INERT	ρ_0 (g/cm^3)	C (mm/μs)	S_1	S_2	S_3	g_0	a
Al 6061	2.703	5.24	1.4	0.0	0.0	1.97	0.48
Teflon	2.15	1.68	1.123	3.983	-5.797	0.59	0.0
Steel	7.90	4.57	1.49	0.0	0.0	1.93	0.5
PMMA	1.182	2.18	2.088	-1.124	0.0	0.85	0.0
Brass	8.45	3.834	1.43	0.0	0.0	2.0	0.0
HDPE	0.954	3.0	1.44	0.0	0.0	1.0	0.0

C-4 REACTIVE FLOW MODELING

Figures 7 – 9 show the calculated pressure histories in the center zone of each Teflon-coated embedded manganin gauge using the Ignition and Growth parameters for C-4 listed in Table 2 and the equations of state for the aluminum flyers and Teflon gauge packages listed in Table 3 for the three disc shaped targets listed in Table 1 in order of increasing shock pressure, These figures also include experimental traces of pressure (solid lines) for a direct comparison between experiment and calculation. Both, measured and calculated growth of reaction in Fig. 7 agree closely for the lowest shock pressure experiment number 4565 listed in Table 1. The transition to detonation occurs just before the 25 mm deep gauge.

For the intermediate shock pressure experiment 4547 shown in Figure 8 good agreement is also demonstrated for the growth of reaction and the transition distance to detonation, which occurs just after the 15 mm deep gauge. For the highest shock C-4 experiment number 4564, the calculated run distance to detonation, which occurs just after the 10 mm deep gauge (Fig. 9), is slightly longer than the experimental run distance of just less than 10 mm. The calculated growth of reaction at the 0 and 5 mm deep gauge positions agrees well with the experimental records. Thus, this relatively simple two-reaction-rate model for C-4 shock initiation agrees quite well with the three sets of pressure history measurements and the run distances to detonation. Further tests of the C-4 parameters can be made if additional experimental data on C-4 becomes available.

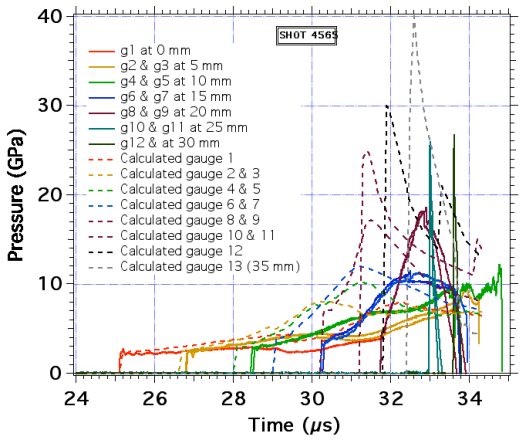

Figure 7. Calculated Pressure Histories for C-4 impacted by an aluminum flyer at 0.6 km/s.

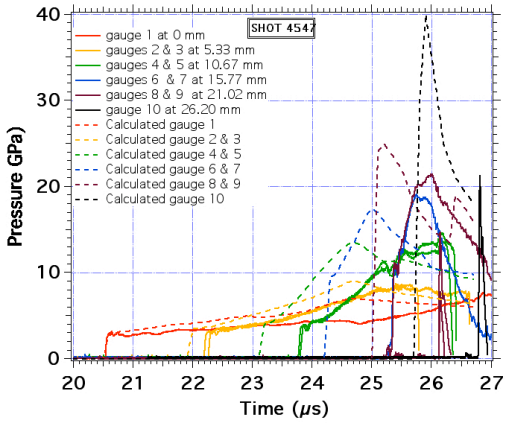

Figure 8. Calculated pressure histories for C-4 impacted by an aluminum flyer at 0.737 km/s.

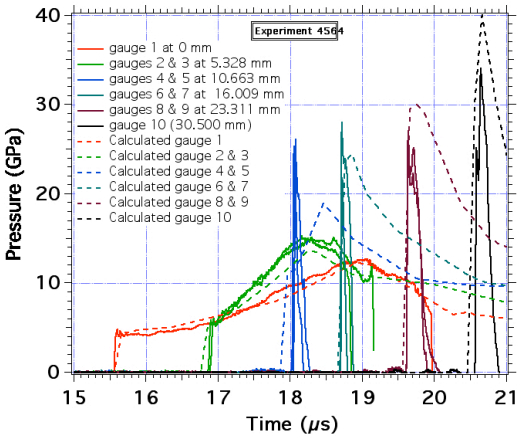

Figure 9. Calculated pressure histories for C-4 impacted by an aluminum flyer at 0.987 km/s.

COMP B REACTIVE FLOW MODELING

Four Comp B embedded gauge experiments using wedge shaped targets are listed in Table 1. The resulting embedded manganin gauge pressure histories and their corresponding calculated pressure histories are shown in Figs. 10 to 13 in order of increasing shock pressure. The model parameters for Comp B are listed in Table 4. For the lowest shock pressure (shot 4359), Fig. 10 shows good agreement for the growth of reaction at the 0, 4.5, 7.75, and 11.01 mm gauge positions and for detonation at the 17.51 mm and 20.77 mm depths. For the next highest shock pressure shot 4544 using an aluminum flyer plate at 0.929 km/s, Fig. 11 shows good agreement between experimental and calculated pressure histories at the first 5 embedded gauges and transition to detonation before the 11.91 and 12.92 mm deep gauges. For the second highest pressure shot 4540, Fig.12 exhibits good agreement between the measured and calculated pressure histories at the first four gauge positions and for detonation at the 10.94 mm and 14.94 mm gauge depths. For the highest shock pressure shot 4545, the measured distance to detonation is slightly less than the 5.47 mm deep gauge position, while the calculated transition occurs just after the 5.47 mm gauge, as shown in Fig. 13. The measured and calculated reaction growths at the 0 mm and 3.58 mm deep gauges agree very well. As mentioned for C-4, a slightly faster transition to detonation rate at high shock pressures is needed for better agreement.

Unlike C-4, Comp B has been used in many shock initiation tests. The more scenarios that a reactive flow model can accurately simulate, then the more useful that model is for safety predictions and design applications. Embedded gauge and laser interferometry experiments provide the most detailed data for shock initiation, but other important tests covering various shock pressure regimes are also used. The following sections contain comparisons between experimental data and Ignition and Growth predictions for several shock initiation scenarios involving Comp B charges.

Table 4. Ignition & Growth parameters for Comp B.

UNREACTED JWL	PRODUCT JWL
A=778.1 Mbar	A=5.242 Mbar
B=-0.05031 Mbar	B=0.07678 Mbar
R_1=11.3	R_1=4.2
R_2=1.13	R_2=1.1
ω=0.8938	ω=0.5
C_V=2.487x10^{-5} Mbar/K	C_V=1.0x10^{-5} Mbar/K
T_O = 298°K	E_O=0.085 Mbar
Shear Modulus=0.0354 Mbar	-
Yield Strength=0.002 Mbar	-
ρ_0=1.717 g/cm^3	-
REACTION RATES	
a=0.0367	x=7.0
b=0.667	y=2.0
c=0.667	z=3.0
d=0.333	F_{igmax}=0.022
e=0.222	F_{G1max}=0.7
g=1.0	F_{G2min} =0.0
I=4.0 x 10^6 μs^{-1}	G_1=140 Mbar^{-2}μs^{-1}
-	G_2=1000 Mbar^{-2}μs^{-1}

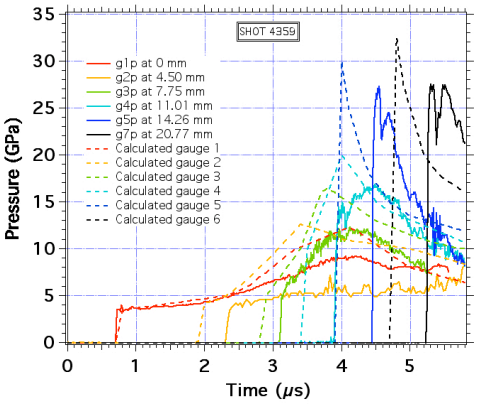

Figure 10. Calculated pressure histories for Comp-B impacted by an aluminum flyer at 0.835 km/s.

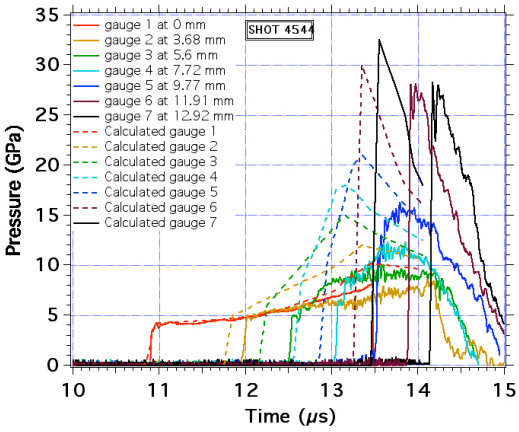

Figure 11. Calculated pressure histories for Comp-B impacted by an aluminum flyer at 0.929 km/s.

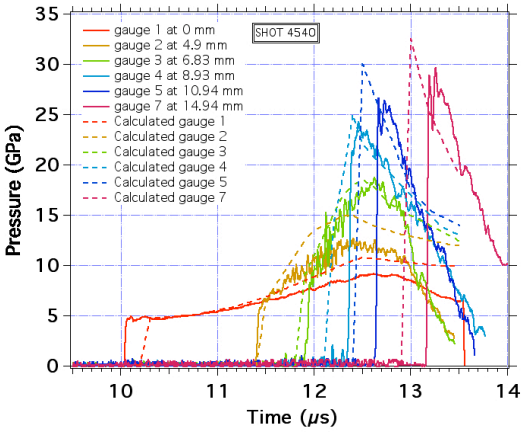

Figure 12. Calculated pressure histories for Comp-B impacted by an aluminum flyer at 1.005 km/s.

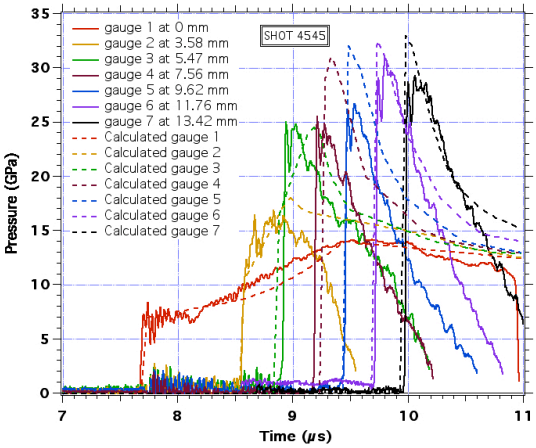

Figure 13. Calculated Pressure histories for Comp-B impacted by an aluminum flyer at 1.307 km/s.

Table 5. Comparisons of Comp B short pulse duration critical velocities

Al Flyer Thickness (mm)	Failure to React / Partial Reaction / Detonation	
	Experimental (km/s)	Calculated (km/s)
0.635 (0.2 μs pulse)	1.1 / 1.5 / 1.6	1.4 / 1.5 /1.6
1.016 (0.3 μs pulse)	--- / 1.1 / 1.2	1.0 / 1.1 /1.2
1.600 (0.5 μs pulse)	0.9 / 1.05 / 1.2	0.85 / 0.95 / 1.1
2.180 (0.7 μs pulse)	0.8 / 0.9 / 1.05	0.7 / 0.85 / 0.95

COMP B SHORT PULSE SHOCK DURATION COMPARISONS

Many intentional and accidental shock initiation scenarios involve short shock pulse durations in which the competition between the ignition and growth of hot spot reactions and the quenching effect of the rarefaction wave following the finite time duration of the initial shock pulse determines whether the explosive charge will detonate. The most familiar and complete study of short pulse duration shock initiation of Comp B is that of Trott and Jung[15] in which several thicknesses of aluminum impacted 20 mm thick Comp B targets at several velocities to determine the critical velocity for shock initiation. The increased run distances to detonation compared to sustained shock pressures were also determined in some cases. The measured failure to initiate / partial reaction / detonation - aluminum flyer velocity data of Trott and Jung for four flyer thicknesses is compared to Ignition and Growth predictions in Table 5. Good agreement is observed especially for the highest shock pressures and shortest duration experiments. The Ignition and Growth calculated run distances to detonation and constant or slightly increasing shock velocities in experiments that did not transition to detonation also agree with Trott and Jung's observations. Since other thin pulse data on different Comp B formulations agree in general with Trott and Jung's data,[16,17] the Comp B parameters appear to be simulating thin pulse initiation well.

COMP B DATA GAP TEST COMPARISONS

The most common type of shock initiation test is the gap test, in which an inert layer of

varying thickness is placed between a donor explosive charge and an acceptor explosive charge. The inert gap thickness is varied until the critical thickness at which 50% of the acceptor charges detonate is determined. Some gap tests are confined by inert walls and some are unconfined. Table 6 lists the 50% detonation gap thicknesses measured for Comp B in five common gap tests: the Pantex Gap Test, which uses an LX-04 donor charge and brass gap material; the Los Alamos National Laboratory (LANL) Small Scale Gap Test (SSGT), which employs a PBX 9407 donor charge and PMMA gap material; the LANL Large Scale Gap Test (LSGT), which uses a PBX 9407 donor charge and aluminum gap material; the Naval Surface Weapons Center (NSWC) SSGT, which uses a PBX 9407 donor charge and PMMA gap material; and the NSWC LSGT, which employs a pentolite donor charge and PMMA gap material. The Pantex Gap and LANL LSGT tests are unconfined, while the others are confined. The confined tests often exhibit more than one regime of shock initiation, because multiple shock waves due to wall reflections are present.[18]

Table 6. C-J Detonation and JWL parameters for donor explosives

Parameter	LX-04 (85% HMX, 15% Viton)	PBX9407 (94% RDX, 6% Exxon 461)	Pentolite (50% PETN, 50% TNT)
ρ_0 (g/cm^3)	1.868	1.60	1.56
D (cm/μs)	0.847	0.791	0.709
P_{CJ} (Mbars)	0.34	0.265	0.205
A (Mbars)	13.3239	5.73187	5.4094
B (Mbars)	0.740218	0.14639	0.093726
R_1	5.9	4.6	4.5
R_2	2.1	1.4	1.1
ω	0.45	0.32	0.35
E_0 (Mbar-cm^3 / cm^3-g)	0.095	0.265	0.042

Finely zoned (10 zones per mm or more), converged two-dimensional Ignition and Growth calculations were done for each of these five gap tests using the Comp B parameters listed in Table 4, the inert equations of state listed in Table 3, and the Chapman-Jouguet (C-J) detonation and Jones-Wilkins-Lee (JWL) equation of state values for the donor explosives listed in Table 6. The calculated ranges of gap thicknesses for no detonation versus detonation of Comp B in these five experiments are listed in Table 7. These calculated ranges of critical gap thickness could be determined more narrowly, but there are all within the experimental gap thickness ranges where some detonations occur.

Since the Comp B tested at various laboratories at different times varies in composition, density, and formulation technique, there is considerable spread in the experimental data. Additionally, since some of the calculated critical gap thicknesses are greater than the experimental 50% points and some are smaller, the agreement between measured and calculated gap thicknesses is reasonable.

Table 7. Comparison of critical gap thicknesses for various gap tests

Gap Test	Experimental 50% Detonation Gap Thickness (mm)	Calculated Gap Thickness (mm)
Pantex	23.2	17-18
NSWC SSGT	4.75	3-4
NSWC LSGT	53.0	50-55
LANL SSGT	0.53	0.3-0.4
LANL LSGT	50.34	55-60

COMPARISONS WITH TWO RECENT PROJECTILE IMPACT EXPERIMENTS

Many studies of shock initiation of bare and covered Comp B charges by projectiles of different materials and geometries have been reported in past years. Two recent studies are modeled in this paper. Lawrence et al.[19] reported critical velocities for shock initiation of 1.717 g/cm^3 Comp B charges 76.2 mm in diameter by 7.62 mm long impacted by right circular mild steel hemispherical cylinders 25.4 mm in diameter and 50.8 mm long. The Comp B charges were either bare or covered by mild steel cover plates 2.38, 4.76, or 9.53 mm thick and were bonded to 25.4 mm thick steel back plates. The projectiles were fired at three angles of obliquity: 0, 30 and 45 degrees. Only the 0° experiments were modeled in finely zoned 2D calculations with the Comp B Ignition and Growth parameters listed in Table 2 and the steel equation of state listed in Table 3. Table 8 lists the measured and calculated critical velocity ranges for shock initiation. The agreement is

excellent and gives confidence in the ability of the model to predict low shock pressure, long run distance to detonation shock initiation threshold in 2D geometries.

The second recent study is that of Almond and Murray,[20] in which flat front brass projectiles of 1.27 cm diameter (0.5 caliber) and 2.24 cm length were fired into 4 cm diameter by 1.2 kg Comp B charges. Critical projectile velocities were determined for bare Comp B and Comp B covered by 1 mm mild steel, 3 mm aluminum, and 5 mm high density polyethlylene (HDPE) discs. Almond and Murray also modeled the shock initiation process in a 2D finite element code using an old two reaction rate Ignition and Growth model for Comp B based on only one set of initiation / no initiation experiments[21] and obtained rather poor agreement with experiment. Table 9 lists the experimental critical velocities and those calculated with the Comp B and inert parameters listed in Tables 2 and 3. Excellent agreement was obtained for bare Comp B charges and those covered with 1 mm of steel and 3 mm of aluminum. The predicted threshold velocity for the 5 mm thick HDPE discs is much higher than the measured value. No details were given concerning the properties of the high density polyethlylene used in the experiments, so perhaps the wrong equation of state and/or density was used in the calculations. Calculations using 5 mm of aluminum instead of HDPE resulted in a critical velocity for shock initiation of 1375 to 1400 m/s, which is close to the experimental threshold of 1348 m/s. Aluminum represents the approximate impedance of a 5 mm inert barrier that would result in predicted prompt shock initiation at the observed velocity. Perhaps a late reaction occurred at lower projectile velocities. However, agreement with the other three critical brass impact velocities is encouraging for the prediction of Comp B shock initiation by the high pressure, short pulse duration shocks produced by small caliber bullets.

Table 8. Comparison of critical steel projectile impact velocities (Ref. 19)

Steel Cover Thickness (mm)	Experimental Velocities (km/s)	Calculated Velocities (km/s)
0.00	1.01 - 1.11	1.05 - 1.10
2.38	1.21 - 1.23	1.15 - 1.20
4.76	1.31 - 1.36	1.25 - 1.35
9.53	1.57 - 1.59	1.45 - 1.50

Table 9. Comparison of critical brass projectile impact velocities (Ref. 20)

Cover Material	Experimental Velocities	Calculated Velocites
Bare Comp B	0.969	0.985-0.989
1 mm Steel	1.086	1.08-1.10
3 mm Aluminum	1.203	1.18-1.20
5 mm HDPE	1.348	1.85

CONCLUSIONS

Embedded manganin pressure gauge records and run distances to detonation were measured at various shock pressures for the RDX-based explosives C-4 and Comp B. These experimental data were used to determine reaction rate parameters for the Ignition and Growth model. The same ignition and growth rate coefficients were used for both explosives. A third reaction rate was then used to simulate the slower TNT reaction rate within the Comp B model. The Comp B parameters were tested against short shock pulse duration, gap test, and projectile impact experimental data with good success. This Comp B model can be used to predict other shock initiation scenarios that have not or can not be experimentally tested directly with a high degree of confidence,

ACKNOWLEDGEMENTS

The authors would like to thank the 101 mm powder gun crew for all their hard work in obtaining the embedded pressure gauge records. This work was performed under the auspices of the United States Department of Energy by the University of California, Lawrence Livermore National Laboratory under Contract No. W-7405-ENG-48.

REFERENCES

1. Forbes, J. W., Tarver, C. M., Urtiew, P. A., and Garcia, F., Eleventh International Detonation Symposium, Office of Naval Research ONR 33300-5, Aspen, CO, 1998, p. 145.

2. Urtiew, P. A., Forbes, J. W., Tarver, C. M., Vandersall, K. S., Garcia, F., Greenwood, D. W., Hsu. P. C., and Maienschein, J. L., Shock Compression of Condensed Matter – 2003, AIP Confernece Proceedings 706, AIP Press, New York, 2004, p. 1053.

3. Trott, B. D. and Jung, R. G., Fifth Symposium (International) on Detonation, Office of Naval Research ACR-184, Pasadena, CA, 1970, p. 191.

4. Cowperthwaite, M. and Rosenberg, J. T., Seventh Symposium (International) on Detonation, Naval Surface Weapons Center NSWC MP 82-334, 1981, Annapolis, MD, p. 1072.

5. Campbell, A. W. and Engelke, R., Sixth Symposium (International) on Detonation, Office of Naval Research ACR-221, Coronado, CA, 1976, p. 642.

6. Tarver, C. M., Erickson, L. M., and Parker, N. L., Shock Waves in Condensed Matter-1983, North Holland Physics Publishing, Santa Fe, NM, 1984, p. 609.

7. Vantine H., Chan J., Erickson L. M., Janzen J., Lee R. and Weingart R. C., "Precision Stress Measurements in Severe Shock-Wave Environments with Low Impedance Manganin Gauges," Rev. Sci. Instr., **51**. pp. 116-122 (1980).

8. P.A. Urtiew, L.M. Erickson, B. Hayes, and N.L. Parker "Pressure and Particle Velocity Measurements in Solids Subjected to Dynamic Loading," Fizika Gorenia i Vzryva, (in Russian) 22, No. 5, pp. 113-126, 1986. Translation in Combustion, Explosion and Shock Waves, 22, No. 5, pp. 597-614, 1986.

9. Vantine, H.C., Erickson, L.M. and Janzen, J., "Hysteresis-Corrected Calibration of Manganin under Shock Loading", J. Appl. Phys., **51** (4), April 1980.

10. Gibbs, T.R. and Popolato, A., LASL Explosive Property Data, p.19, University of California Press, Berkeley, CA, 1980.

11. Tarver, C. M., Lefrancois, A. S., Lee, R. S. and Vandersall, K. S., "Shock initiation of the PETN-based Explosive LX-16," paper presented at this Symposium.

12. Campbell, A. W. and Travis, J. R., "The Shock Desensitization of PBX 9404 and Composition B-3," Eighth Symposium (International) on Detonation, Naval Surface Weapons Center NSWC 86-194, Albuquerque, NM, 1985, p. 1057.

13. Tarver, C. M., Erickson, L. M. and Parker, N. L., "Shock Initiation, Detonation Wave Propagation and Metal Acceleration Measurements and Calculations for RX-26-AF," Shock Waves in Condensed Matter – 1983, J. R. Asay, R. A. Graham, and G. K. Straub, eds., North Holland Physics Publishing, Amsterdam, 1984, p. 609.

14. Tao, W. C., Tarver, C. M., Kury, J. W., Lee, C. G. and Ornellas, D. L."Understanding Composite Explosive Energetics IV: Reactive Flow Modeling of Aluminum Reaction Kinetics in PETN and TNT Using Normalized Product Equation of State," Tenth International Detonation Symposium, Office of the Chief of Naval Research OCNR 33395-12, Boston, MA, 1993, p. 628.

15. Trott, B. D. and Jung, R. G., "Effect of Pulse Duration on the Impact Sensitivity of Solid Explosives," Fifth Symposium (International) on Detonation," Office of Naval Research ACR-184, Pasadena, CA, 1970, p. 191.

16. de Longueville, Y., Fauquignon, C., and Moulard, H., "Initiation of Several Condensed Explosives by a Given Duration Shock Wave," Sixth Symposium (International) on Detonation, Office of Naval Research ACR-221, Coronado, CA, 1976, p. 105.

17. Moulard, H., "Critical Conditions for Shock Initiation of Detonation by Small projectile Impact," Seventh Symposium (International) on Detonation, Naval Surface Weapons Center NSWC MP 82-334, Annapolis, MD, p. 316.

18. Tarver, C. M. and James, E., "Two-Dimensional Reactive Flow Modeling of the Minimum priming Charge, LANL Large Scale Gap and NOL Large Scale Gap Test," JANNAF Propulsion Hazards Meeting, Monterey, CA, February 1986.

19. Lawrence, W., Krzewinski, B., Starkenberg, J., and Baker, P., "Projectile-Impact Shock-Initiation Experiments and CTH Simulation Comparisons," Army Research Laboratory Report ARL-RP-116, Aberdeen Proving Ground, MD, February 2006.

20. Almond, R. J. and Murray, S. G., "Projectile Attack of Surface Scattered Munitions: Prompt Shock Finite Element Models and Live Trials," Propellants, Explosives, Pyrotechnics **31**, 83 (2006).

21. Murphy, M. J., Lee, E. L., Weston, A. M. and Williams, A. E., "Modeling Shock Initiation in Composition B," Tenth International Detonation Symposium, Office of the Chief of Naval Research OCNR 33395-12, Boston, MA, 1993, p. 963.